

PACS numbers: 07.57.Hm; 07.57.Pt; 07.57.Ty; 74.25.–q
DOI: 10.1070/QE2007v037n10ABEH013614

Terahertz BWO spectroscopy of conductors and superconductors

B.P. Gorshunov, A.A. Volkov, A.S. Prokhorov, I.E. Spektor, J. Akimitsu, M. Dressel, G.J. Nieuwenhuys, S. Tomić, S. Uchida

***Abstract*. Methods for direct (without the use of the Kramers–Kronig relations) measuring the dielectric response (dynamic conductivity and permittivity) spectra of dielectrics, conductors, and superconductors in the terahertz frequency range (0.03–1.5 THz) are described. The methods are realised by using BWO (backward-wave oscillator) spectrometers developed at the A.M. Prokhorov General Physics Institute, RAS. Dielectric measurements can be performed at temperatures from 2 to 1000 K in magnetic fields up to 8 T. The dielectric response spectra are investigated for a number of materials with properties determined by electron correlation effects: superconductors, one-dimensional conductors, heavy fermion systems, spin-ladder cuprates, and spin glasses.**

Keywords: *terahertz spectroscopy, electron correlations, low temperatures*.

1. Introduction

Electron correlations are a central topic of the modern condensed matter physics and provide the basis for a wide variety of fundamental physical phenomena such as superconductivity, charge and magnetic orderings, plasmon excitations, phase transitions, heavy fermions, intermediate valence, and charge and spin density waves. A specific feature of systems with collectivised electrons is that the typical energies characterising their ground state, such as the energy gap of superconductors, the plasma oscillation energy, relaxation energies of quasiparticles and a hybridisation gap in heavy fermion compounds, the pinning energy of charge/spin density waves, etc., are comparatively small (of the order of a few millielectronvolts). This leads to certain difficulties in the solution of fundamental and applied problems related to the experimental study of correlated electron systems because the use of modern spectroscopic methods, especially optical spectroscopy in such a low-energy region involves serious problems.

The corresponding frequency range, approximately between 10^{11} and 10^{12} Hz, has even been called the 'spectroscopic gap' ('submillimetre gap' or 'terahertz gap') by researchers working in the field of optical spectroscopy. Progress in the experimental studies in the terahertz frequency range was achieved in recent years due to the use of a new generation of quasi-optical spectrometers developed at the A.M. Prokhorov General Physics Institute and based on monochromatic radiation sources – backward-wave oscillators (BWOs) [1].

Modern BWO spectrometers provide rapid and reliable measurements of the dielectric response of materials at frequencies in the range from 1 to 50 cm^{-1}, which corresponds to photon energies 0.15–6 meV. The mastering of the 'terahertz gap' not only raised optical spectroscopy to a new level of panoramic dielectric measurements [2] but also opened up the possibilities for solving many fundamental and applied problems by using experimental data obtained in the previously inaccessible spectral region.

In this paper, we describe recent advances in the development of methods for terahertz dielectric measurements of conducting and superconducting materials and also present recent results obtained by the method of terahertz BWO spectroscopy for compounds with strong electron correlations: one-dimensional conductors, superconductors, systems with heavy fermions, spin-ladder cuprates, and spin glasses. If necessary, to investigate phenomena more completely, the BWO measurements were supplemented with data obtained in an extended frequency range by using microwave and infrared spectrometers. At the same time, the data acquired at terahertz frequencies were of key importance for obtaining a number of new physical results.

2. Measurement of the dielectric response spectra of conducting materials in the terahertz frequency range

The operation principle of BWO spectrometers in a standard configuration is described in detail in a number of papers (see, for example, [1, 3–5]). Briefly, it is based on the measurement of the transmission Tr(ν) and phase shift $\varphi(\nu)$ spectra of a wave propagated through a plane–parallel

B.P. Gorshunov, A.A. Volkov, A.S. Prokhorov, I.E. Spektor
A.M.Prokhorov General Physics Institute, Russian Academy of Sciences, ul. Vavilova 38, 119991 Moscow, Russia; e-mail: gorshunov@ran.gpi.ru;
J. Akimitsu Department of Physics, Aoyma-Gakuin University, Tokyo, Japan; e-mail: jun@phys.aoyama.ac.jp;
M. Dressel 1. Physikalisches Institut, Universität Stuttgart, Stuttgart, Germany; e-mail: dressel@pil.physik.uni-stuttgart.de;
G.J. Nieuwenhuys Kemerlingh Onnes Laboratory, Leiden University, Leiden, The Netehrlands; e-mail: gerard.nieuwenhuys@psi.ch;
S. Tomić Institut za Fiziku, HR-100001 Zagreb, Croatia;
e-mail: stomic@ifs.hr;
S. Uchida Department of Physics. University of Tokyo, Tokyo, Japan; e-mail: uchida@phys.s.u-tokyo.ac.jp

Received 2 May 2007
Kvantovaya Elektronika **37** (10) 916–923 (2007)
Translated by M.N. Sapozhnikov

plate made of a material under study (Fig. 1a). Then, by using standard Fresnel formulas for the transmission coefficient of a layer (see, for example, [6]), the spectra of the optical parameters of a sample such as the permittivity $\varepsilon^*(\nu) = \varepsilon'(\nu) + i\varepsilon''(\nu)$, conductivity $\sigma^*(\nu) = \sigma'(\nu) + i\sigma''(\nu)$, refractive index $n^*(\nu) = n(\nu) + ik(\nu)$, etc. are calculated. Optical parameters measured with BWO spectrometers are determined by solving a system of two equations for two unknowns, for example, n and k (Fig. 1). It is important that the parameters of the sample are calculated directly, without the use of integral Kramers–Kronig relations, which are employed in IR Fourier spectroscopy measurements. In the latter case, the reflection spectrum $R(\nu)$ of the sample surface is measured, and to obtain dielectric parameters, it is necessary to analyse the spectrum $R(\nu)$ by using the Kramers–Kronig relation, which introduces specific uncertainties due to the extrapolation of $R(\nu)$ outside the frequency region in which the measurements were performed.

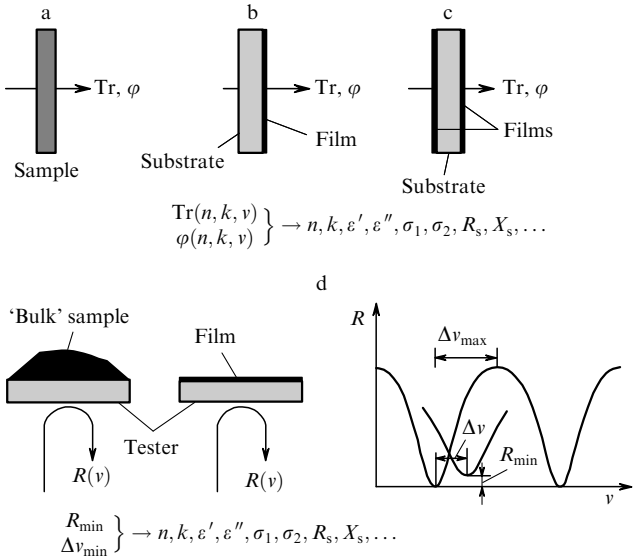

Figure 1. Schemes for determining terahertz dielectric spectra of materials from the measured transmission spectra Tr and phase shift φ of a wave propagated through a plane–parallel sample (a), one (b), and two (c) thin films on dielectric substrates, and the scheme for measuring the terahertz dielectric parameters of strongly absorbing materials by the dielectric tester method (d). In the latter case, parameters are calculated by using the measured variations in the frequency and magnitude of the interference minimum in the reflection spectrum caused by a contact of the tester with the sample under study.

Note, however, that the use of the above-described standard BWO spectroscopy for studying conducting materials involves serious difficulties. The problem appears due to their low transparency because it is necessary to prepare samples with an unrealistic small thickness (less than micrometer) for reliable measurements of transmission coefficients. To provide BWO-spectroscopy measurements of weakly trans-parent materials (conducting and superconducting), we developed special procedures based on the measurement of the spectra of the complex transmission coefficient of films on dielectric substrates and reflection spectra from a 'bulk' sample or an etalon transparent plane–parallel plate with a sample pressed to it on the rear side (with respect to incident radiation). Both these procedures provide measurements of the optical parameters of samples directly without using Kramers–Kronig relations.

2.1 Measurement of terahertz dielectric spectra of conducting films on dielectric substrates

Studying films on substrates (Fig. 1b) makes sense either when the sample can be principally prepared in the form of a thin film or when studying a non-transparent material it is impossible to prepare a thin enough film whose properties are close to those of a bulk material. In principle, the terahertz measurements of films on dielectric substrates are similar to the measurements of single-layer samples. They involve the measurement of the transmission coefficient and phase shift of a wave propagated through a two-layer film-on-substrate system, followed by the calculation of the dielectric parameters of the films by using the corresponding Fresnel formulas for a two-layer medium [6]. It is obvious that the optical parameters of a transparent substrate should be measured preliminarily by using the standard procedure [1, 3–5] (Fig. 1a).

As an example Figs 2a, c show the measured temperature dependences of the terahertz conductivity and permittivity of a niobium nitrid (NbN) superconducting film on a sapphire substrate [7]. One can see that this method provides the measurement of the electrodynamic parameters of conducting films in the normal phase with good accuracy. At the same time the accuracy of measuring the dynamic conductivity σ' in the superconducting state strongly decreases. This is typical for superconducting film samples, whose transmission coefficient and phase shift at frequencies $\nu < 2\Delta/h$ (2Δ is the superconducting gap) are mainly determined by the permittivity, which can achieve large negative values: in the given case, $\varepsilon' \approx -10^6$ at $T =$

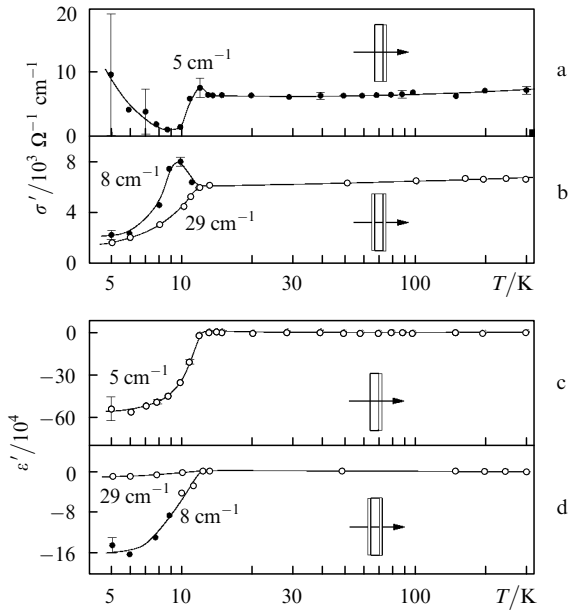

Figure 2. Temperature dependences of the dynamic conductivity and permittivity of a superconducting NbN film determined from the measured transmission coefficient and phase shift of a wave propagated through a sample for one 115-Å-thick NbN film on a 0.43-mm-thick sapphire substrate (a, c) and two NbN films (540 Å) deposited on both sides of a 0.39-mm sapphire substrate (b, d). The measurement errors of ε' in the normal phase correspond to the size of experimental points [7].

5 K. The accuracy of measuring σ' of a superconductor can be improved by depositing thin films of a material under study on both sides of a transparent substrate (Fig. 1c). Such a system represents a Fabry–Perot resonator, and the sensitivity is increased due to the high Q of the resonator, especially in the superconducting state, when absorption (conductivity σ') in 'mirrors' (films) decreases and, therefore, the efficiency of radiation interaction with films increases. This is demonstrated by the temperature dependences of σ' and ε' for a NbN film in Figs 2b, d, which were determined from the transmission spectra and the phase shift of a wave transmitted through a substrate with two films deposited on both sides: instead of the uncertain behaviour of the conductivity in the superconducting state in the case of one film (Figs 2a, c), the decrease in σ' is reliably observed at lowest temperatures and the characteristic peak is observed at a low frequency (8 cm^{-1}) slightly below the critical temperature.

2.2 Measurement of terahertz reflection spectra

If it is impossible to prepare a thin enough film with properties close to those of a bulk sample and transparent enough for reliable dielectric measurements in the transmission geometry to be performed, reflection is measured either from the surface of a bulk sample or from an etalon transparent plane–parallel plate ('dielectric' tester) with a sample pressed to it on the rear side (with respect to incident radiation).

2.2.1. Measurement of the reflection spectra of a bulk sample

The measurement of the reflection coefficient of a plane surface of a 'semi-infinite' sample, especially at low temperatures in a cryostat, is a rather challenging problem. The matter is that, to determine the reflection spectrum $R(\nu) = I_{sam}(\nu)/I_m(\nu)$, it is necessary to measure separately the radiation intensity reflected from a sample (I_{sam}) and from a reference (metal) mirror (I_m), i.e. the procedure involves the replacement of the sample by the mirror in the measuring aperture. The experimental terahertz spectra $I_{sam}(\nu)$ and $I_m(\nu)$ are inevitably distorted by standing waves appearing due to multiple reflections of radiation between the sample (or mirror) and elements of the quasi-optical measuring system (cryostat windows, polarisers, lenses, attenuators, etc.) Therefore, if the sample is replaced by the mirror not accurately enough, these standing waves are not cancelled in the calculated $R(\nu)$, and distortions up to a few tens of percent can appear in the spectrum $R(\nu)$.

We developed systems providing the replacement of the sample by the mirror in a quasi-optical cryostat with accuracy sufficient for reliable measurements of the terahertz reflection spectra of conductors or superconductors at a level exceeding 95 %, up to 99 %. Figure 3 shows an example of such spectra measured for a single crystal of a high-temperature $La_{1.88}Sr_{0.12}CuO_4$ superconductor [8]. The spectra were measured at different temperatures (in the superconducting and normal phases) for two polarisations: $\boldsymbol{E} \parallel \boldsymbol{c}$, when the radiation electric field vector is directed along the c axis, i.e. perpendicular to the CuO planes, and $\boldsymbol{E} \perp \boldsymbol{c}$. The measurements were performed down to low frequencies ($\sim 1-2$ cm^{-1}), where distortions caused by standing waves are strongest. For $\boldsymbol{E} \perp \boldsymbol{c}$, the reflection coefficient is high both in the normal and superconducting phases. For $\boldsymbol{E} \parallel \boldsymbol{c}$, the $La_{1.88}Sr_{0.12}CuO_4$ crystal is a 'poor conductor' in the normal phase: the reflection coefficient is small and is ~ 50 % for $\nu > 20$ cm^{-1}; for $\nu < 20$ cm^{-1}, the Hagen–Rubens behaviour of the reflection coefficient is observed: $R \to 100$ %, which is caused by a finite (although small) static conductivity [9]. The spectra in the superconducting phase exhibit a plasma edge related to the plasma oscillations of Cooper pairs, which are delocalised in the direction of the c axis due to tunnelling through Josephson weak links between the CuO planes. In this case, the reflection coefficient becomes almost equal to 100 % at frequencies below 10–20 cm^{-1}.

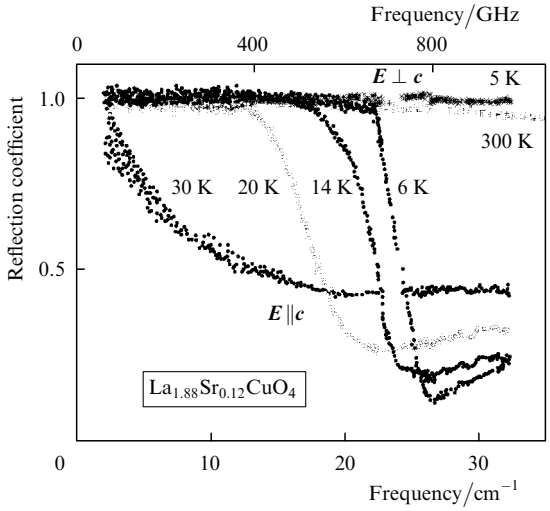

Figure 3. Terahertz reflection spectra of a $La_{1.88}Sr_{0.12}CuO_4$ single crystal measured at different temperatures for polarisation $\boldsymbol{E} \parallel \boldsymbol{c}$, when the electric field vector $\boldsymbol{E}$ is perpendicular to superconducting CuO planes, and for $\boldsymbol{E} \perp \boldsymbol{c}$, when the vector $\boldsymbol{E}$ is parallel to superconducting planes [8].

The information on the electrodynamic parameters of a bulk sample can be obtained from its reflection spectra either by processing $R(\nu)$ with the use of the known dispersion mechanisms or by measuring the spectrum with a Fourier spectrometer in a broader range and analysing it with the help of the Kramers–Kronig relations. The key moment in this case is that BWO spectrometers provide the high absolute accuracy of measuring terahertz spectra $R(\nu)$, which cannot be obtained with Fourier spectrometers and is ± 0.3 % for $R = 99$ %. This is illustrated by the results presented in paper [10], where the reflection spectra of a high-temperature $La_{1.88}Sr_{0.12}CuO_4$ superconductor in the terahertz region 8–33 cm^{-1} were obtained at different temperatures and supplemented with IR measurements in the range from 30 to 30000 cm^{-1}. Analysis of the combined terahertz and IR spectra $R(\nu)$ by using the Kramers–Kronig relations gave quantitative information on the London penetration depth and on the fulfilment of the sum rule for the spectral weight in the superconducting and normal phases.

2.2.2. Dielectric tester method

This method allows one to determine the electrodynamic parameters of conducting materials directly, i.e. without using the Kramers–Kronig relations. The reflection coefficient of a tester in the form of a plane–parallel transparent plate with the known dielectric properties is measured in the experiment (Fig. 1d). This spectrum contains periodic minima appearing due to the interference of radiation

inside the tester. If a sample is pressed to the rear face of the tester, the conditions of reflection from this face change, resulting in a change (shift) $R_{\min}$ of the amplitude (depth) and the frequency position $\Delta\nu$ of each of the interference minima. The measurement of these two shifts allows one to calculate the two unknown characteristics of the sample. Figure 4a presents the terahertz dielectric spectra of liquids measured by the dielectric tester method [11]. This method is attractive because in this case there is no need to use special cells. Figure 4b shows that this method can be also used to measure the dielectric response of films on substrates, when the film parameters cannot be measured in transmission. One can see from this figure that, by using a silicon tester, it is possible to measure the dynamic conductivity of even a metal (gold) film, for which $\sigma' \approx 3.5 \times 10^5\ \Omega^{-1}\ \mathrm{cm}^{-1} \pm 30\,\%$ for $\nu = 10\ \mathrm{cm}^{-1}$.

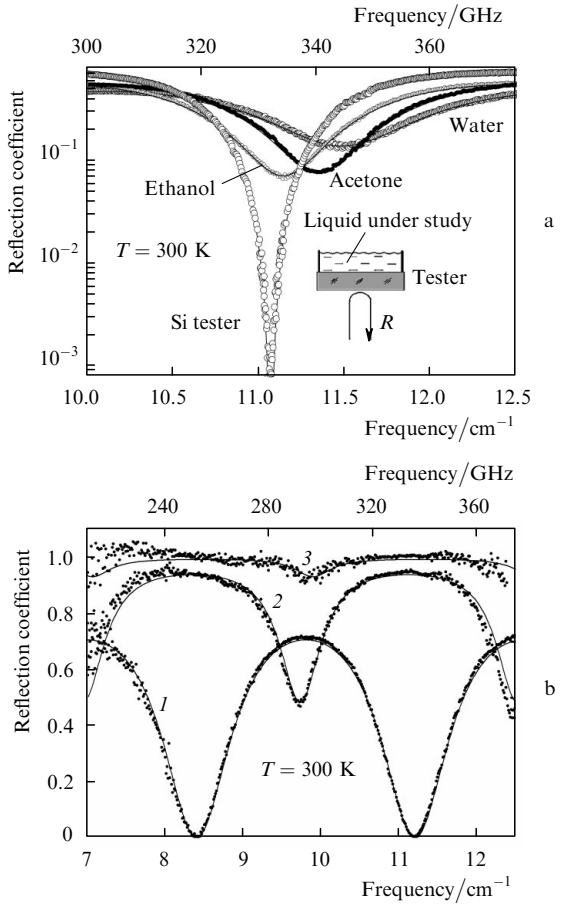

Figure 4. Interference minima in the terahertz reflection spectra (circles) of a plane–parallel highly-insulating silicon plate (dielectric tester) with different liquids under study; the solid curves are the least-square fits applied to determine the dielectric parameters of liquids (a) [11], and also the reflection spectra of a 0.525-mm thick plane–parallel silicon substrate (*1*) and the same substrate with a 50-nm-thick conducting AuFe film (*2*) and a 50-nm-thick Au film (3); points are experiment; the solid curves are the least-square fits using the expressions for the reflection coefficient of single- and two-layer media (b) [40].

3. Terahertz spectroscopy of conductors with electron correlations

Below, we present briefly the results of some terahertz BWO-spectroscopy studies of dielectric properties of materials containing correlated electron subsystems (one-dimensional conductors, high-temperature superconductors, heavy fermions, spin-ladder cuprates, and spin glasses) performed at the GPI, RAS.

3.1 Manifestation of fluctuations of charge density waves in terahertz spectra of one-dimensional conductors

Effects caused by charge density waves (CDWs) play the most important role in the electronic properties of one-dimensional conductors. The CDW is a collective electron–phonon formation produced due to the Fermi surface 'nesting' [12, 13]: in a one-dimensional conductor in the case of finite electron–phonon interaction, the state in which a superstructure and the related redistribution of the positive ion charge appear in the ion lattice is advantageous in energy. The excess ion positive charge is screened by conduction electrons, resulting in the formation of a CDW. The CDW dynamics is related to a peculiar collective type of conductivity in solids: electron charge clusters can move in an external electric field, thereby carrying a current; in this case, positive ions remain at their places, and oscillates about their equilibrium positions. Charge density wave fluctuations at temperatures $T > T_{\mathrm{MF}}$ play an important role in conductivity processes (T_{MF} is the temperature of transition to the CDW phase in the mean-field approximation).

We measured the terahertz spectra of several one-dimensional conductors. The dielectric spectra exhibited some specific features directly related to CDW fluctuations. Figure 5 shows the spectra of the dynamic conductivity of one-dimensional $K_{0.3}MoO_3$ and $(TaSe_4)_2I$ conductors [14, 15]. Along with a strong anisotropy, the spectra in the case of longitudinal polarisation ($E_\parallel$) exhibit absorption bands at $\sim 3\ \mathrm{cm}^{-1}$ caused by CDW fluctuations. These

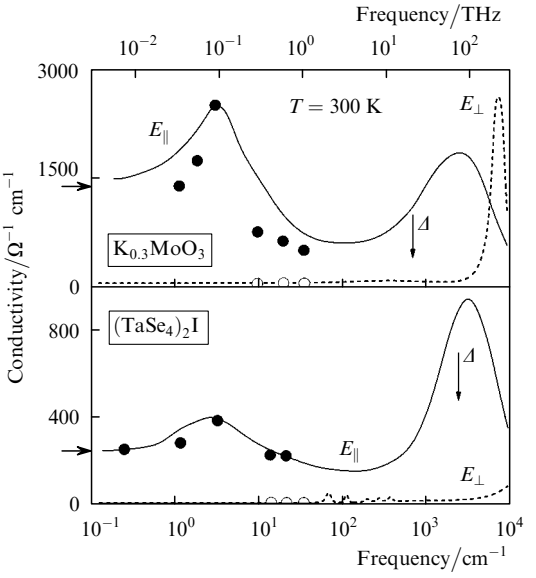

Figure 5. Frequency dependences of the conductivity of one-dimensional conductors $K_{0.3}MoO_3$ and $(TaSe_4)_2I$ for the longitudinal ($E_\parallel$, dark circles) and transverse ($E_\perp$, light circles) polarisations. The vertical arrows show the positions of Peierls CDW gaps calculated from the activation behaviour of the static conductivity. The horizontal arrows indicate the values of static conductivities. The solid curves are the least-square fits describing the absorption line by the Lorentz model and the 'through' conductivity by the Drude model [14, 15].

bands are related to the segments of fluctuating CDWs, which experience a local pinning giving rise to resonance absorption. At the same time, the thermal energy causes a partial depinning of CDWs, resulting in the appearance of a finite collective Drude contribution to the static conductivity (the horizontal arrows in Fig. 5).

3.2 Anomalous absorption of electromagnetic radiation in the superconducting phase of high-temperature superconductors

The measurement of the optical response of high-temperature superconductors (HTSCs) at frequencies $v < 2\Delta/h$ gives information on the fundamental properties of the superconducting state such as the order parameter symmetry, the magnitude and temperature dependence of the London penetration depth, the nature of the 'residual' absorption (for $T \ll T_c$, where T_c is the superconducting transition temperature), the type of scattering of quasiparticles, the possible collective modes, etc. After the discovery of HTSCs, when the preparation of high-quality samples suitable for BWO-spectroscopy studies was worked out, we performed the first measurements of the terahertz spectra of the dielectric response in HTSC cuprates of different compositions and immediately obtained the result which proved to be related to the specificity of the superconducting state in the whole HTSC class. The result consists in the 'anomalous' (compared to the BCS superconductors) behaviour of the absorption of electromagnetic radiation. While absorption of radiation in the superconducting phase of a BCS superconductor decreases [16], it strongly increases in HTSCs (Fig. 6) [17, 18].

One can see from Fig. 6 that for $T < T_c$, the permittivity decreases down to large negative values; such a behaviour of $\varepsilon'(T)$ is universal for superconductors and corresponds to the inductive response of the condensate of Cooper pairs

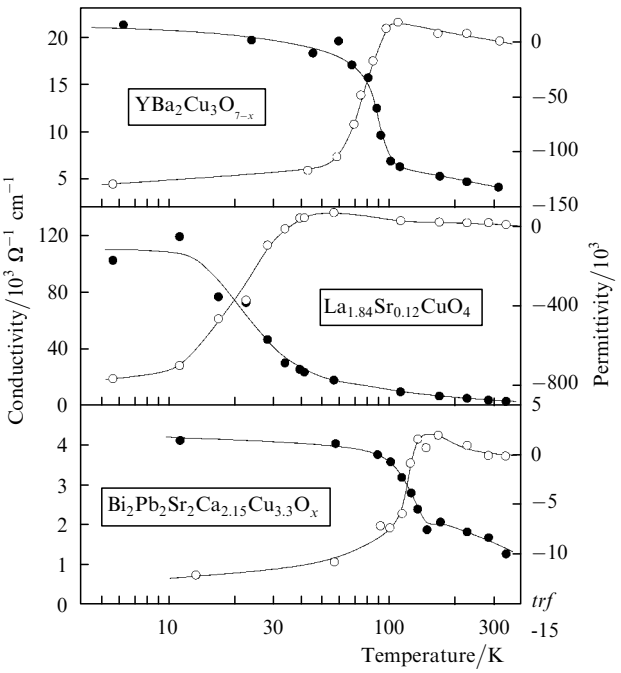

Figure 6. Temperature dependences of the dynamic conductivity (dark circles) and permittivity (light circles) of HTSC cuprates $YBa_2Cu_3O_{7-x}$ (at a frequency of 0.27 THz), $La_{1.84}Sr_{0.12}CuO_4$ (0.17 THz), and $Bi_2Pb_2Sr_2Ca_{2.15}Cu_{3.3}O_x$ (0.36 THz) measured with a BWO spectrometer.

located 'under' the delta function at the zero frequency in the spectrum of the conductivity $\sigma'(T)$ [16]. Simultaneously, the conductivity in the superconducting phase considerably increases, which is caused by the presence of quasiparticles in HTSC cuprates even at the lowest temperatures. Later, we observed additional absorption in the superconducting state also in high-quality single-crystal HTSC samples [19, 20]. Moreover, it is established now that the residual absorption in the IR – terahertz regions is present virtually in all HTSC cuprates.

It seems that the origin of quasiparticles is related to the d-type of the order-parameter symmetry. Indeed, the gap of the d symmetry in HTSCs vanishes in certain regions of the Fermi surface [21, 22]. Then, 'thermally-induced' quasiparticles should be present in the system at any finite temperature, which will inevitably cause the additional 'residual' absorption in the superconducting state. Note also that quasiparticles can be produced in a HTSC due to the formation of 'stripes' and the local suppression of superconductivity by impurities, for example, zinc.

3.3 Transverse Josephson plasmon in a T*-cuprate $SmLa_{0.85}Sr_{0.15}CuO_{4-\delta}$

The electrodynamic properties of HTSC cuprates in the direction perpendicular to the CuO planes, i.e. along the c axis, also attract great attention. The plasma oscillations of a condensate of Cooper pairs along the c axis (Josephson plasmons) are of interest because, on the one hand, they allow one to study the mechanism of superconductivity in cuprates since the behaviour of transverse plasmons is determined by the microscopic characteristics of the electron condensate such as its compressibility, concentration, and conductivity. The electrodynamic properties of cuprates in transverse polarisation are also important for studying the energetics of the superconducting transition [23, 24]. On the other hand, the layer structure of cuprates can produce special types of collective excitations in the superconducting phase. For example, in cuprates with the two types of insulating layers between the CuO planes in the unit cell for $\boldsymbol{E} \parallel \boldsymbol{c}$, along with two longitudinal plasma modes, one transverse plasma mode should be observed – in fact a new type of collective excitation in layered superconductors, which was predicted in theoretical paper [25]. We observed such excitation for the first time in the terahertz spectra of a $SmLa_{0.85}Sr_{0.15}CuO_{4-\delta}$ single-crystalline sample [26]. Figure 7 shows the corresponding results. One can see that two maxima in the loss function spectrum and a maximum in the conductivity spectrum are observed upon transition to the superconducting state; the corresponding dispersion is also observed in the permittivity spectra. The temperature evolution of the maxima allows us to reliably assign these maxima to two longitudinal and one transverse plasma oscillations, respectively. Excitations observed at terahertz frequencies are well described qualitatively and quantitatively by microscopic models considering the delocalisation of charge carriers (Cooper pairs) in the superconducting phase due to their tunnelling through Josephson weak links (of two types) between the CuO planes [27, 28].

3.4 Nature of heavy quasiparticles in heavy fermion UPd_2Al_3 and UPt_3 compounds

The interaction of conduction electrons with localised magnetic moments in heavy fermion (HF) compounds

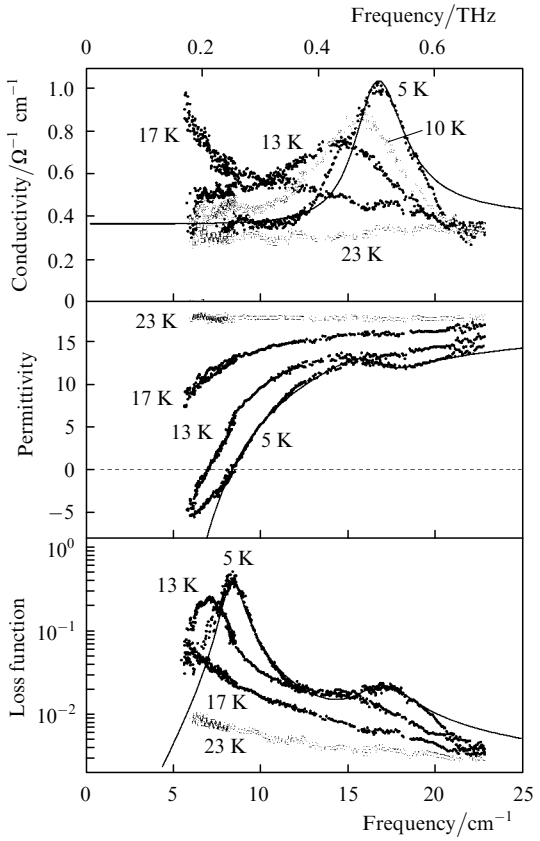

Figure 7. Terahertz spectra of the conductivity, permittivity, and the loss function of a $SmLa_{0.85}Sr_{0.15}CuO_{4-\delta}$ single crystal measured for the $\boldsymbol{E} \parallel \boldsymbol{c}$ polarisation at different temperatures [8]. The solid curves are constructed by using the model from [25].

leads to the formation of the correlated ground state whose properties can be described by the Landau Fermi liquid theory with the effective mass of quasiparticles achieving several hundreds and thousands of free electron masses. One of the most interesting problems in the physics of HF materials is the coexistence of the HF condensate and the superconductivity of heavy quasiparticles with the magnetic ordering. At first glance, the establishment of the magnetic order should suppress both the transition to the regime of coherent scattering of mobile electrons by the localised moments of the Kondo lattice accompanied by the formation of heavy quasiparticles and the pairing of individual fermions in a Cooper pair. Nevertheless, a number of uranium-based HF compounds exist in which the superconductivity of 'heavy Cooper pairs' not only 'gets along with' the magnetic phase, but moreover, as accepted now, magnetic excitations are intermediaries in the Cooper pairing of quasiparticles [29, 30]. If the interaction between the electron and magnetic subsystems facilitates the appearance of the superconducting state in HF compounds, the question appears about the role of such an interaction in the nonsuperconducting phase as well.

We studied the dynamics of quasiparticles coexisting with the magnetic order in the UPd_2Al_3 ($T_N = 14$ K, $T_c = 2$ K) and UPt_3 ($T_N = 5$ K, $T_c = 0.5$ K) compounds [31]. The results obtained for UPd_2Al_3 (the data for UPt_3 are qualitatively similar) are illustrated in Fig. 8. For $T = 300$ K, the spectra have the form typical of a Drude metal [9]. As temperature is decreased, the low-frequency conductivity increases, which corresponds to the appearance of a narrow Drude component of heavy quasiparticles. For $T < T_N$, a rather narrow gap (~ 0.2 meV) appears in the conductivity spectra. Analysis shows [31] that this gap in UPd_2Al_3 (and in UPt_3) appears due to the interaction of the electron condensate with the antiferromagnetic ordered phase and the formation of heavy particles in the ground state should be caused by the interaction of mobile electrons with the magnetic phase.

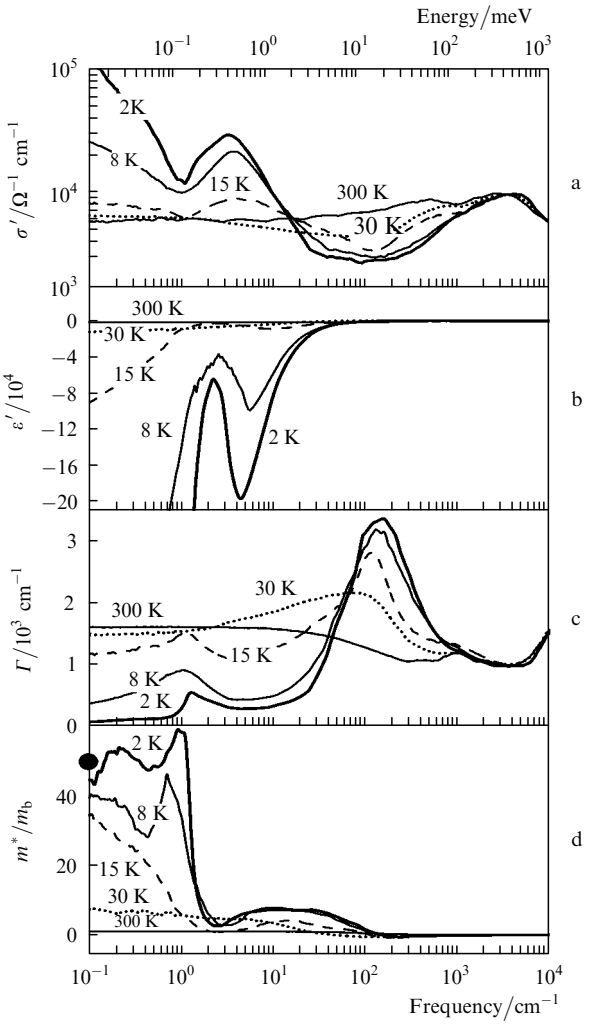

Figure 8. Frequency dependences of the conductivity (a), permittivity (b), scattering rate (c), and effective mass (d) of an UPd_2Al_3 compound at different temperatures (m_b is the band electron mass) [31]. The dark circle on the vertical axis in Fig. 8d corresponds to the effective mass obtained from thermodynamic measurements.

3.5 Detection of a charge density wave in a spin-ladder cuprate $Sr_{14-x}Ca_xCu_{24}O_{41}$

In low-dimensional systems (one- or two-dimensional), a competition between different collective ground states of the electron subsystem, for example, between superconductivity and CDWs can be observed [32]. Such a competition should be demonstrated, in particular, by a family of spin-ladder $Sr_{14-x}Ca_xCu_{24}O_{41}$ cuprates [33]. These cuprates consist of spin CuO_2 chains and Cu_2O_3 ladders, the conductivity being carried out through a subsystem of ladders doped with holes. This material

attracts attention because it is the first superconducting cuprate with a non-square (one-dimensional) crystal lattice. As shown theoretically in [34], in a doped system representing a 'two-leg spin ladder', a spin gap should appear due to the localisation of holes on individual rungs, which can be in fact the pairing mechanism and could lead to superconductivity; it was also shown in [34] that the superconducting instability will compete with the CDW instability. The superconductivity of this compound was later observed (with $T_c \approx 10$ K at a pressure of several GPa) [35] and its nature is still a matter of active discussions.

We performed dielectric measurements in a broad spectral range and discovered for the first time the phase transition to the CDW state predicted theoretically [36]. Figure 9 shows the typical spectra for polarisation along 'ladder legs'. The figure demonstrates the appearance of the CDW gap, the pinning CDW phason, and a broad-range temperature-dependent response at radio frequencies. We showed that this phase transition has a number of parameters that are unusual for typical dimensional conductors. In particular, this is the transition of the semiconductor–semiconductor type rather than of the metal–conductor type, and it is characterised by the absence of nonlinear conductivity and a small CDW effective mass. We also found for the first time that the substitution of strontium by calcium in $Sr_{14-x}Ca_xCu_{24}O_{41}$, which is required to obtain superconductivity, suppresses the CDW phase. The inset in Fig. 9 shows the phase diagram constructed for the CDW, which demonstrates the competing character of the superconducting and CDW phases in $Sr_{14-x}Ca_xCu_{24}O_{41}$ (Fig. 9).

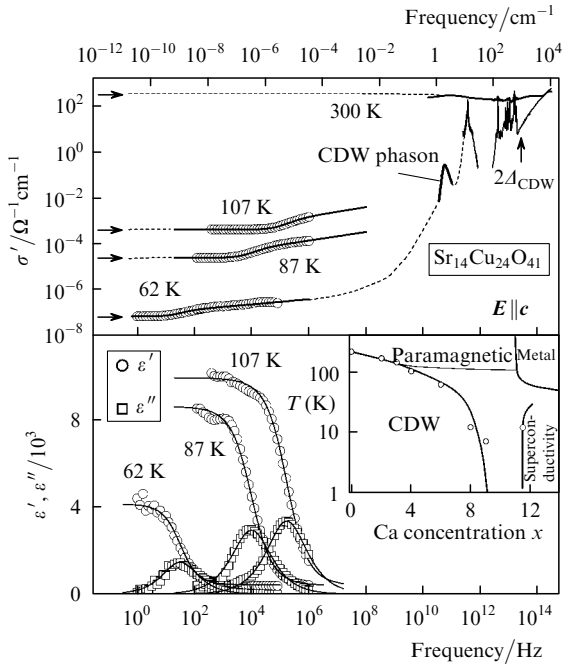

Figure 9. Conductivity and permittivity spectra of a $Sr_{14}Cu_{24}O_{41}$ single crystal measured at different temperatures along the conducting axis ($E \| c$). The arrows show the static conductivity, the solid curves are the spectra constructed by using the generalised Drude model; the dashed curves are drawn for convenience. The maximum at a frequency of 2 cm^{-1} is taken from [37, 38]. The inset shows the phase diagram for $Sr_{14-x}Ca_xCu_{24}O_{41}$ constructed by using the experimental panoramic dielectric spectra of the compound.

3.6 The RKKY interaction and electron localisation in a AuFe spin glass

Processes proceeding in spin glasses are a central theme in modern solid-state physics [39]. In these materials, a new magnetic state of matter is in fact realised, whose properties are of fundamental interest and can find important practical applications. Although spin glasses have been studied in many theoretical and experimental papers, there is no consensus on the nature of the spin-glass state. Because the exchange Ruderman–Kittel–Kasuya–Yosida (RKKY) interaction of spins via the subsystem of mobile electrons is the fundamental phenomenon in the physics of the spin-glass state, it is obvious that the properties of the electron subsystem should be intimately related with the formation and stabilisation of the low-temperature glass phase. An important factor preventing an understanding of the properties of the electron subsystem is the absence of optical spectroscopic data for spin glasses, which can give fundamental information about microscopic parameters of the electronic subsystem. We have measured for the first time the electrodynamic response of AuFe spin glasses by the methods of terahertz BWO spectroscopy, infrared Fourier spectroscopy, and optical ellipsometry [40]. In the spin-glass phase at 5 K, the conductivity dispersion was found at frequencies 10–40 cm^{-1} that is caused by the mobility gap appearing in the subsystem of free electrons involved in the RKKY interaction between magnetic Fe centres (Fig. 10). Moreover, variations in the microscopic parameters (relaxation frequency and time, plasma frequency, and conductivity) of charge carriers in Au films after the addition of Fe due to scattering by magnetic moments were determined quantitatively.

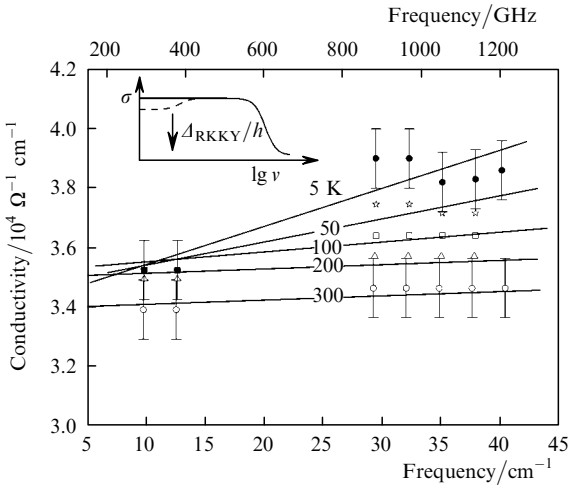

Figure 10. Frequency dependences of the conductivity of a 50-nm-thick $Au_{1-x}Fe_x$ film (the atomic concentration is $x = 6\%$) measured at different temperatures. The solid auxiliary lines demonstrate a noticeable frequency dependence of the conductivity at temperatures below 100 K. The solid curves in the inset show schematically the frequency dependence of the free-electron conductivity, the dashed curve shows how the conductivity spectrum is modified due to the RKKY interaction between magnetic impurities via free electrons accompanied by the formation of a gap at frequencies below Δ_{RKKY}/h (Δ_{RKKY} is the characteristic energy of the RKKY interaction) [40].

Acknowledgements. This work was supported by the Russian Foundation for Basic Research (Grant Nos 05-02-

16490-a, 06-02-16010-a) and the Program for Fundamental Research 'Problems of Radiophysics' of the Department of Physical Sciences, RAS.

References

1. Kozlov G., Volkov A., in *Millimeter and Submillimeter Spectroscopy of Solids* (Topics in Applied Physics, vol. 84) Ed. by G. Grüner (Berlin – Haidelberg: Springer, 1998) p. 51.
2. Volkov A.A., Prokhorov A.S. *Izv. Vyssh. Uchebn. Zaved., Ser. Radiofiz.*, **XLVI**, 732 (2003).
3. Kozlov G.V., Prokhorov A.M., Volkov A.A., in *Problems of Solid State Physics*. Ed. by A.M. Prokhorov, A.S. Prokhorov (Moscow: Mir Publishers, 1984).
4. Volkov A.A., Goncharov Yu.G., Kozlov G.V., Lebedev S.P., Prokhorov A.M. *Infrared Phys.*, **25**, 369 (1985).
5. Volkov A.A., Kozlov G.V., Prokhorov A.M. *Infrared Phys.*, **29**, 747 (1989).
6. Born M., Wolf E. *Principles of Optics* (Oxford: Pergamon Press, 1969; Moscow: Nauka, 1973).
7. Volkov A.A., Gorshunov B.P., Kozlov G.V., Fedorov I.V., Semenov A.D. *Zh. Eksp. Teor. Fiz.*, **104**, 2546 (1993).
8. Gorshunov B., Volkov A., Spektor I., Prokhorov A., Mukhin A., Dressel M., Uchida S., Loidl A. *Int. J. Infrared Millimeter Waves*, **26**, 1217 (2005).
9. Sokolov A.V. *Opticheskie svoistva metallov* (Optical Properties of Metals) (Moscow: Fizmatgiz, 1961).
10. Tajima S., Fudamoto Y., Kakeshita T., Gorshunov B., Zelezny V., Kojima K.M., Dressel M., Uchida S. *Phys. Rev. B*, **71**, 094508 (2005).
11. Spektor I., Anzin V., Goncharov Yu., Gorshunov B., Gusev G., Komandin G., Lebedev S., Volkov A., in *Proc. the Joint 30th Intern. Conf. on Infrared and Millimeter Waves and 13th Intern. Conf. on Terahertz Electronics* (USA, Williamsburg, Virginia, 2005).
12. Peierls R.E. *Quantum Theory of Solids* (Oxford: Clarendon Press, 1955; Moscow: Inostrannaya Literatura, 1956).
13. Frohlich H. *Proc. Roy. Soc. A*, **223**, 296 (1954).
14. Gorshunov B.P., Volkov A.A., Kozlov G.V., Degiorgi L., Blank A., Csiba T., Dressel M., Kim Y., Schwartz A., Gruner G. *Phys. Rev. Lett.*, **73**, 308 (1994).
15. Schwartz A., Dressel M., Alavi B., Blank A., Dubois S., Gruner G., Gorshunov B.P., Volkov A.A., Kozlov G.V., Thieme S., Degiorgi L., Levy F. *Phys. Rev. B*, **52**, 5643 (1995).
16. Tinkham M. *Introduction to Superconductivity* (New York: McGraw-Hill, 1975).
17. Gorshunov B.P., Pronin A.V., Volkov A.A., Somal H.S., van der Marel D., Feenstra B.J., Jaccard Y., Locquet J.-P. *Physica B*, **244**, 15 (1998).
18. Pronin A.V., Gorshunov B.P., Volkov A.A., Somal H.S., van der Narel D., Feenstra B.D., Jakkard Y., Loke J.P. *Pis'ma Zh. Eksp. Teor. Fiz.*, **68**, 406 (1998).
19. Schutzmann J., Gorshunov B., Renk K.F., Munzel J., Zibold A., Gezerich H.P., Erb A., Muller-Vogt G. *Phys. Rev. B*, **46**, 512 (1992).
20. Tajima S., Fudamoto Y., Kakeshita T., Gorshunov B., Zelezny V., Kojima K.M., Dressel M., Uchida S. *Phys. Rev. B*, **71**, 094508 (2005).
21. Hardy W.N., Bonn D.A., Morgan D.C., Liang R., Chang K. *Phys. Rev. Lett.*, **70**, 3999 (1993).
22. Maksimov E.G. *Usp. Fiz. Nauk*, **170**, 1033 (2000).
23. Anderson P.W. *Science*, **268**, 1154 (1995).
24. Basov D.N., Woods S.I., Katz A.S., Singley E.J., Dynes R.C., Xu M., Hinks D.G., Homes C.C., Strongin M. *Science*, **283**, 49 (1999).
25. Van der Marel D., Tsvetkov A.A. *Czech. J. Phys.*, **46**, 3165 (1996).
26. Kakeshita T., Uchida S., Kojima K.M., Adachi S., Tajima S., Gorshunov B., Dressel M. *Phys. Rev. Lett.*, **86**, 4140 (2001).
27. Van der Marel D., Tsvetkov A. *Phys. Rev. B*, **64**, 024530 (2001).
28. Helm Ch., Bulaevsky L.N., Maley M.P. *Phys. Rev. Lett.*, **89**, 057003 (2002).
29. Thalmeier P., Zwicjnagel G., in *Handbook on the Physics and Chemistry of Rare Earths* (Amsterdam: Elsevier, 2004) Vol. 34, Chap. 219.
30. Mathur N.D., Grosche F.M., Julian S.R., et al. *Nature*, **394**, 39 (1998).
31. Dressel M., Kasper N., Petukhov K., Gorshunov B., Gruner G., Huth M., Adrian H. *Phys. Rev. Lett.*, **88**, 186404 (2002).
32. Emery V.J., in *Highly Conducting One-dimensional Solids*. Ed. by J. Devreese, R. Evrard, V. van Doren (New York: Plenum Press, 1979) p. 247.
33. Dagotto E. *Rep. Prog. Phys.*, **62**, 1525 (1999).
34. Dagotto E., Riera J., Scalapino D. *Phys. Rev. B*, **45**, 5744 (1992).
35. Uehara M., Nagata T., Akimitsu J., Takahashi H., Mori N., Kinoshita K.J. *Phys. Soc. Jpn.*, **65**, 2764 (1996).
36. Gorshunov B., Haas P., Rõõm T., Dressel M., Vuletic T., Hamzic B., Tomic S., Akimitsu J., Nagata T. *Phys. Rev. B*, **66**, 060508 (2002).
37. Kitano H., Isobe R., Hanaguri T., et al. *Europhys. Lett.*, **56**, 434 (2001).
38. Vuletic T., Korin-Hamzic B., Ivek T., Tomic S., Gorshunov B., Dressel M., Akimitsu J. *Phys. Reports*, **428**, 169 (2006).
39. Mydosh J.A. *Spin Glasses, an Experimental Introduction* (London: Taylor and Francis, 1993).
40. Gorshunov B., Prokhorov A.S., Kaiser S., Faltermeier D., Yasin S., Dumm M., Drichko N., Zhukova E.S., Spektor I.E., Vongtragol S., Hesselberth M.B.S., Aarts J., Neuwenhuys G.J., Dressel M. *Europhys. Lett.*, **76**, 938 (2006)